Polymer 50 (2009) 3609–3616

Contents lists available at ScienceDirect

Polymer

journal homepage: www.elsevier.com/locate/polymer

Surface mechanical properties of transparent poly(methyl methacrylate)/zirconia nanocomposites prepared by *in situ* bulk polymerization

Yiqing Hu, Shuxue Zhou*, Limin Wu

Department of Materials Science and Advanced Coatings Research Center of Educational Ministry of China, Fudan University, Shanghai 200433, P.R. China

ARTICLE INFO

Article history:
Received 25 September 2008
Received in revised form
18 December 2008
Accepted 8 March 2009
Available online 26 March 2009

Keywords:
Poly(methyl methacrylate)
Zirconia nanoparticles
Mechanical property

ABSTRACT

Poly(methyl methacrylate)/zirconia (PMMA/ZrO_2) nanocomposites with ZrO_2 content as high as 15 wt% were prepared by modifying non-aqueous synthesized ZrO_2 nanoparticles with methacryloxypropyltrimethoxysilane (MPS) in tetrahydrofuran, dispersing MPS-functionalized ZrO_2 nanoparticles in MMA and following *in situ* bulk polymerization with controlled pre-polymerization time. The MPS-functionalized ZrO_2 nanoparticles showed an efficient crosslinking role in the polymerization, leading to a complete gel of PMMA at 5 wt% of ZrO_2 content. Homogeneous dispersion of the ZrO_2 nanoparticles at primary particle size level was observed in all nanocomposites, which results in good clarity of the obtained nanocomposites. Hardness tests (pendulum hardness tests and indentation tests) and anti-scratch tests (abrasion tests and nano scratch tests) were employed to probe the surface mechanical properties of the nanocomposites. The properties of nanocomposites as a function of ZrO_2 content, revealing from various characterization techniques, are not consistent and discussed in detail. At low ZrO_2 content, the mechanical properties are enhanced by the formed crosslinking structure. However, remarkable improvements of hardness and scratch resistance of PMMA were achieved when 15 wt% of ZrO_2 content was embedded.

1. Introduction

Poly(methyl methacrylate) (PMMA) is a typical transparent amorphous polymer and has been widely used as an important material for optical devices. PMMA has several advantages of good flexibility, high strength and excellent dimensional stability, however, suffers from the shortcomings such as poor heat resistance, weak mechanical surface, low refractive index, etc. [1,2]. In the past decade, inorganic nanoparticles (or nanophase materials) are incorporated into PMMA to overcome its drawbacks or to render it with new optical functionality. For examples, SiO_2 [3], TiO_2 [3–6], ZnO [3,7], ZrO_2 [3,8], AlN [3] nanoparticles as well as clay [9] were undergone surface treatment and embedded into PMMA via *in situ* polymerization [3–7,9] or solution blending method [8] to improve the thermal stability of PMMA. Alumina nanoparticles coated with 3-glycidoxypropyltrimethoxysilane was used to get PMMA/alumina nanocomposites displaying a room-temperature brittle-to-ductile transition [10]. Calcium carbonate nanopowder, modified with stearic acid, was incorporated into PMMA via *in situ* polymerization to improve the abrasion resistance of PMMA [11]. Methacryloxypropyltrimethoxysilane (MPS)-modified colloidal silica nanoparticles can increase the hardness of PMMA coating from 3H to 5H [12]. Enhanced hardness as well as tensile strength and tensile modulus were also demonstrated in MPS-grafted silica nanopowder reinforced PMMA [13] and increased tensile strength and tensile modulus reported in PMMA/clay nanocomposites [9]. Transparent luminescent PMMA/ZnS:Mn nanocomposites were obtained by the bulk polymerization of transparent dispersions containing manganese-doped ZnS nanoparticles [14] while PMMA/ZnO nanocomposites with UV-absorption and moderately high refractive index were prepared via *in situ* bulk polymerization in the presence of tert-butylphosphonic acid-modified ZnO nanoparticles [15]. The other nanophase materials reported for the preparation of PMMA-based nanocomposites include palladium nanoparticles [16], $Ni_{0.5}Zn_{0.5}Fe_2O_4$ nanoparticles [17], C_{60} [18] and so on. Although PMMA-based nanocomposites have been widely investigated, there are two deficiencies in this research area. One aspect lies in the insufficient evaluation of the surface mechanical properties which are critical for practical application of the nanocomposites such as optical lens. Another aspect is stemmed from the fabrication process. It could be easily seen that *in situ* bulk polymerization was frequently used in the fabrication of PMMA-based nanocomposites. To improve the compatibility of nanoparticles with PMMA matrix and meanwhile avoid the influence of

* Corresponding author. Tel.: +86 21 55664030; fax: +86 21 55664033.
E-mail address: zhoushuxue@fudan.edu.cn (S. Zhou).

0032-3861/$ – see front matter © 2009 Elsevier Ltd. All rights reserved.
doi:10.1016/j.polymer.2009.03.028

nanoparticles on the polymerization of MMA, ligands with inert character in radical polymerization are grafted onto the nanoparticles in most cases. With this kind of surface modification aggregation of nanoparticles upon polymerization easily takes place due to depletion force and thus reduces the transparency of PMMA-based nanocomposite especially at high nanoparticle load [3,7,15].

Zirconia (ZrO_2) material has advantages of chemical inertness, excellent thermal stability, high refractive index and high hardness. The nano-sized zirconia has been successfully used to fabricate nanocomposite coatings with high hardness [19], high refractive index [20–22] and improved scratch resistance [23]. ZrO_2 nanopowder was used to reduce the thermal expansion coefficient of poly(ether-sulfone) for meeting its application in the connector of optical fiber [24] while colloidal ZrO_2 sols, prepared from reverse emulsion technique, were found to increase the dielectric permittivity of conductive polymer [25–27]. ZrO_2 nanophase material has also been combined with PMMA matrix [3,8,28,29]. However, most of the studies [3,8,28] focused on the thermal stabilities and seldom on the surface mechanical properties of the PMMA/ZrO_2 nanocomposites.

In this work, highly crystalline ZrO_2 nanoparticles, synthesized from a solvothermal reaction of zirconium-(IV) isopropoxide isopropanol complex in benzyl alcohol [30], were employed to fabricate PMMA/ZrO_2 nanocomposites. These non-aqueous synthesized ZrO_2 nanoparticles are highly dispersible in organic solvents as well as in MMA with the aid of ligands, as described in our previous publications [31,32]. They had been successfully utilized to fabricate transparent photopolymerized nanocomposites for volume holographic gratings with the highest refractive index contrast (n1 of up to 0.024) [30] as well as for scratch resistant nanocomposite coatings for polycarbonate [23]. Herein the non-aqueous synthesized ZrO_2 nanoparticles were modified with MPS and dispersed in MMA. Highly transparent PMMA/ZrO_2 nanocomposites with ZrO_2 content as high as 15 wt% were successfully prepared via *in situ* bulk polymerization of the MMA/ZrO_2 dispersions with controlled pre-polymerization time. Their surface mechanical properties, such as hardness, scratch resistance, probed with various techniques were especially paid attention to. Besides the acquisition of PMMA sheets with enhanced mechanical surface, this study also sheds light on the structure–hardness–scratch resistance relationship of nanocomposites.

2. Experimental section

2.1. Materials

Zirconium(IV) isopropoxide isopropanol complex (99.9%) and anhydrous benzyl alcohol (≥99%,) were purchased from Aldrich. Tetrahydrofuran (THF, ≥99.5%), MMA were the products of Sinopharm Chemical Reagent Corp. MPS (≥98%) was obtained from Sigma. Azo-bisisobutyronitrile (AIBN) was purchased from Shanghai Guanghua Chemical Reagent Corp. (China), which was recrystallized in ethanol before use.

2.2. Synthesis of ZrO_2 nanocrystals

The synthesis of ZrO_2 nanocrystals was described in detail elsewhere [32]. Zirconium (IV) isopropoxide isopropanol complex (3.33 g) and 50 mL of anhydrous benzyl alcohol were weighed into a 100-ml Teflon-lined autoclave. The Teflon-lined autoclave was sealed and put in oven, and then heated to 240 °C. After 4 days, the reaction mixture was cooled down, and a white turbid liquid suspension was obtained. X-ray diffraction analysis indicated that the solid product is cubic single-crystal ZrO_2 nanoparticles with high crystallinity [30,31].

2.3. Functionalization of ZrO_2 nanocrystals with MPS

As-synthesized ZrO_2 nanoparticle suspension was centrifuged to remove benzyl alcohol, and then washed with absolute ethanol by two cycles of sonication and centrifugation. The wet ZrO_2 nanoparticles were dispersed in the pre-made THF/MPS solution to achieve a solid content of 15 mg/g based on MPS-to-ZrO_2 molar ratio of 0.2:1. The dispersion was sonicated at room temperature for 20 min and put in an oven with temperature of 60 °C for 20 h. Afterwards, the dispersion was concentrated to a ZrO_2 concentration of about 200 mg/g by a rotary evaporator, then precipitated with a large amount of methanol. The precipitate was washed with methanol twice to remove the free MPS molecules, and dried under vacuum at room temperature for 30 min.

2.4. Preparation of PMMA/ZrO_2 nanocomposites slice

A certain amount of MPS-functionalized ZrO_2 nanoparticles was mixed with MMA (about 18 ml) and sonicated at ambient temperature for 20 min. The obtained MMA/ZrO_2 dispersion was kept overnight. Another sonication of 20 min was carried out before polymerization. The initiator, AIBN (0.06 wt% based on the weight of MMA), was added into the dispersion. The polymerization reaction was conducted at 75 ± 2 °C under mechanical stirring until the reactant attained a desired viscosity. Then, the viscous prepolymer was transferred into a glass mold and kept at 40 °C for 24 h and 100 °C for 1 h to complete the polymerization. PMMA/ZrO_2 nanocomposite slices were obtained by disassembling the mold.

2.5. Characterization

Thermogravimetric analysis (TGA) was carried out using a Perkin Elmer TGA-7 instrument (USA) at a heating rate of 10 °C/min in air. The solid-state ^{29}Si NMR spectra were acquired by a Bruker DMX500 spectrometer (Germany) equipped with a 4-mm MAS probe head.

Transmission electron microscopy (TEM Hitachi H-600 instrument, Hitachi Corp., Japan) was used to observe the morphology of nanocomposites. The specimens were prepared using an ultramicrotome. Thin sections of about 50 nm were cut from the nanocomposite slices without further staining. The gel fraction and the polymerization conversion of the nanocomposites were determined by Soxhlet extracting experiments using THF as the solvent with 48 h of reflux. The gel fraction was calculated by the mass of the nanocomposite remained after extraction (M_1) dividing the initial mass of the nanocomposite (M_0). However, the mass of the free PMMA chains dissolved in THF (M_2) was counted in the calculation of polymerization conversion (C), and therefore the polymer conversion was obtained according to the equation, $C = (M_1 + M_2)/M_0$. The UV/vis transmission spectra were obtained with a UV-1800PC spectrophotometer (Shanghai Mei-Pu-Da Instrument Corp., Ltd., China). The transmission data at a wavelength of 550 nm were adopted.

The pendulum hardness of the nanocomposites was measured with the 707 KP pendulum hardness rocker (Sheen Instrument Ltd., UK). The time of the Koenig-pendulum swing from 6° to 3° was automatically recorded at 20 °C. The average value from three measurements on different sites of the same sample was adopted. Indentation tests were performed on a CSEM Indenter (SA Corporation, Switzerland). A three-side pyramid diamond indenter was employed. Loading and unloading rates were set as 33 nm/s and holding time as 5 s. The maximum load applied was 20 mN. Before

each indentation measurement, the tip was calibrated with a standard quartz (reduced elastic modulus 69.6 GPa). Unloading curves were used to analyze the elastic modulus and the hardness of the samples.

The scratch resistance was evaluated by two methods: abrasion experiments and nano scratch tests. The former was conducted on a 5131 abrader (Taber, USA) at 20 °C using a CS-10 abrasion wheel, 500 g load and 20 cycles. The optical transmissions before (T_0) and after (T_1) abrasion were measured with a UV-1800PC spectrophotometer (Shanghai Mei-Pu-Da Instrument Corp., Ltd., China) at a wavelength of 550 nm. The reduction of transparency (ΔT) was calculated by the equation:

$$\Delta T = \frac{T_0 - T_1}{T_0} \times 100\% \quad (1)$$

The lower value of ΔT means a better scratch resistance of the sample. Nano scratch test was conducted using a Nano Indenter XP system (MTS Systems Corporation, USA). A Berkovich diamond tip with a diameter of 2 μm was used. An initial surface profile of the samples was detected by a pre-scan procedure with a minimum load of 0.1 mN. After that, the tip was pushed with increasing load from 0 to 100 mN into the sample, and moved with a constant velocity of 10 μm/s. The surface profile was recorded by a depth sensor. A post-scan was performed to determine the deformation recovery and the residual depth of the scratch after the diamond tip was removed. Three parallel scratches were carried out for each sample and average values were adopted.

3. Results and discussion

3.1. Preparation of MPS-functionalized ZrO_2 nanoparticles

The dispersion of ZrO_2 nanoparticles in MMA without any agglomeration was demonstrated [31] using MPS as the ligand. In this work, MPS-functionalized ZrO_2 nanoparticles were first prepared in THF and free MPS molecules were removed by precipitation with methanol. The critical factors influencing the dispersion and functionalization of ZrO_2 nanoparticles in THF are the molar ratio of MPS-to-ZrO_2 and ZrO_2 concentration [23]. A least MPS-to-ZrO_2 molar ratio of 0.11:1 to achieve a ZrO_2 nanoparticle dispersion at primary particle size level was ever indicated in our previous studies [31]. Herein, the MPS-to-ZrO_2 molar ratio of 0.2:1 was adopted to guarantee the rapid attaching of MPS. With this MPS-to-ZrO_2 molar ratio, the effect of ZrO_2 concentration on the preparation of transparent ZrO_2 dispersion was investigated. A transparent ZrO_2 dispersion was reached after 5 min of sonication at 1.5 wt% of ZrO_2 concentration but after 20 min of sonication at 2.0 wt% of ZrO_2 concentration. When the ZrO_2 concentration was further increased to 6 wt%, completely transparent ZrO_2 dispersion was not obtained no matter how long the sonication process was, implying that some ZrO_2 nanoparticles may turn into hard aggregates. The great impact of ZrO_2 concentration on the dispersing of ZrO_2 nanoparticles has been explained by the colliding probability of nanoparticles and the easier water adsorption of non-aqueous synthesized ZrO_2 nanoparticles in the air [23]. Therefore, a lower ZrO_2 concentration, 1.5 wt%, was selected during modification process to avoid the formation of ZrO_2 aggregates.

In addition, we surprisingly found that the ZrO_2 dispersion would transform into translucency after about 6 h of magnetic stirring at 60 °C. As a consequence, the MPS-functionalized ZrO_2 nanoparticles are poorly dispersible in MMA. This phenomenon is opposite to the common viewpoint that stirring help the dispersion of nanoparticles, and the reason is just studying under way. To make sure the better dispersion of the MPS-modified ZrO_2 nanoparticles in MMA the surface modification process was undergone without stirring. The modification time also impact the dispersion of MPS-functionalized ZrO_2 nanoparticles in MMA to some extent. A cursory investigation suggested that 20 h of modification time would be preferred.

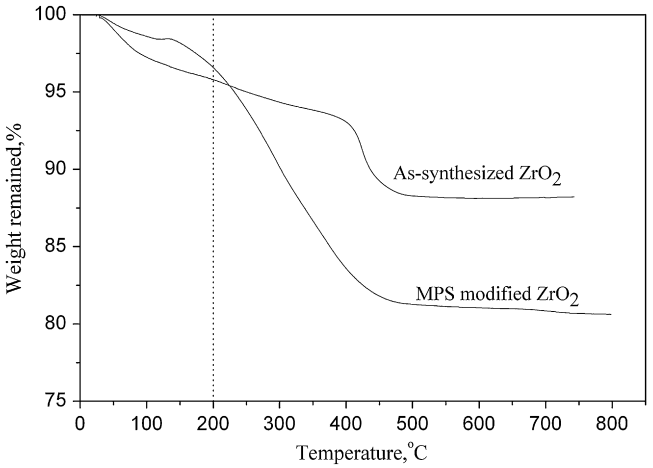

Fig. 1. TGA curves of the as-synthesized ZrO_2 and MPS-functionalized ZrO_2 nanocrystals.

Therefore, the optimized process for the preparation of MPS-functionalized ZrO_2 nanoparticles would be as follows: MPS-to-ZrO_2 molar ratio 0.2:1, ZrO_2 concentration 1.5 wt%, sonication time 20 min at room temperature, heating time: 20 h at 60 °C, and no stirring. The corresponding MPS-functionalized ZrO_2 nanoparticles were characterized by TGA, as shown in Fig. 1. The TGA curve of the as-synthesized ZrO_2 nanoparticles is also presented in Fig. 1. Clearly, MPS-functionalized ZrO_2 nanoparticles have an increased weight loss relative to as-synthesized ZrO_2 nanoparticles, which is attributed to the organic components of the attached MPS. The ^{29}Si NMR spectrum of the MPS-modified ZrO_2 nanoparticles is presented in Fig. 2. The signals at 49.7 ppm, 55.9 ppm and 63.8 ppm corresponding to the T^1, T^2 and T^3 structure are all observed, suggesting that MPS molecules was attached to ZrO_2 nanoparticles based on the bonding fashions shown in Scheme 1. To our surprise, the signal at 42.2 ppm due to T^0 structure is also clearly exhibited, although the sample has been washed with methanol four times before measurement. The T^0 structure may be resulted either from the remained free MPS molecules or from the MPS molecules that were attached to ZrO_2 nanoparticles via coordination of C = C bond

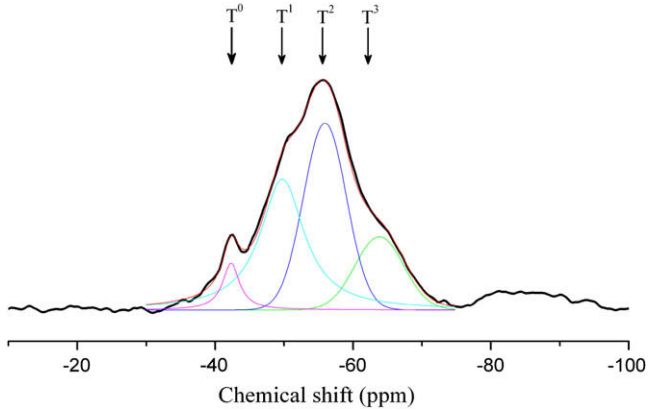

Fig. 2. ^{29}Si NMR spectrum of MPS-modified ZrO_2 nanoparticles.

with the exposed zirconium atom (see Scheme 1). Combining TGA results with ^{29}Si NMR spectrum, the amount of the attached MPS can be calculated as 16.0 g/100 g ZrO_2, namely 62.4 C = C bonds attached to each ZrO_2 nanoparticle (size: 3.8 nm).

3.2. Preparation of PMMA/ZrO_2 nanocomposites *via* in situ polymerization

In situ bulk polymerization was employed to prepare PMMA/ZrO_2 nanocomposites in this work because bulk polymerization is an industrial process for preparation of optical PMMA sheet. With this method, fabrication of transparent MMA/ZrO_2 dispersion is critical to acquire transparent PMMA/ZrO_2 nanocomposite. Fortunately, the obtained MPS-functionalized ZrO_2 nanoparticles are quite "soluble" in MMA. Transparent ZrO_2/MMA dispersion can be obtained even at ZrO_2 concentration of 20 wt% via simple sonication, as shown in Fig. 3. An as-synthesized ZrO_2/MMA dispersion was also given in the figure for comparison.

Similar to the common bulk polymerization of MMA, *in situ* bulk polymerization of MMA/ZrO_2 dispersion was also conducted by two steps: pre-polymerization under stirring and subsequent polymerization in a glass mold. As we know, a proper viscosity attained by pre-polymerization step is paramount for a bulk polymerization process. Table 1 summarizes the pre-polymerization time to reach a desired viscosity (0.9 Pa s) for the MMA/ZrO_2 dispersions containing various ZrO_2 contents. As the ZrO_2 content increases, the pre-polymerization time increases at a ZrO_2 content up to 3 wt%, and then quickly shortens at high ZrO_2 load level. The above change of pre-polymerization time with ZrO_2 load could be explained by the immobilized MPS segments on the surface of ZrO_2 nanoparticles which can participate in the copolymerization. The MPS radicals, initiated or transferred, were less active both in propagation and in termination reaction due to the restricted diffusion.

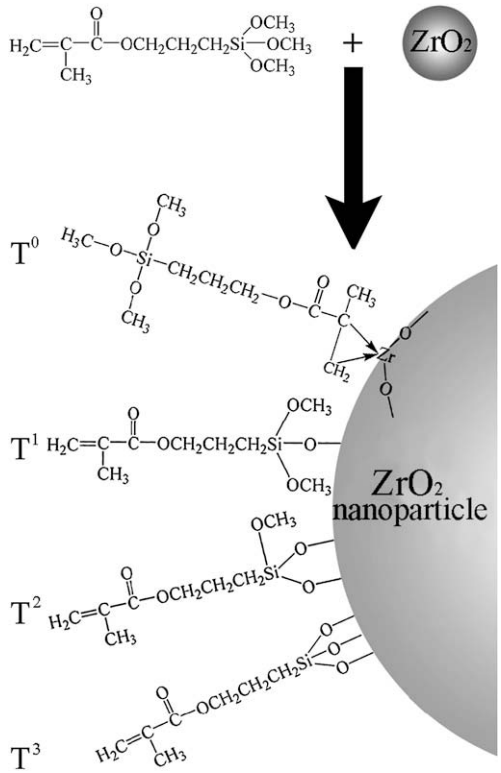

Scheme 1. The bonding fashions of MPS with ZrO_2 nanoparticles.

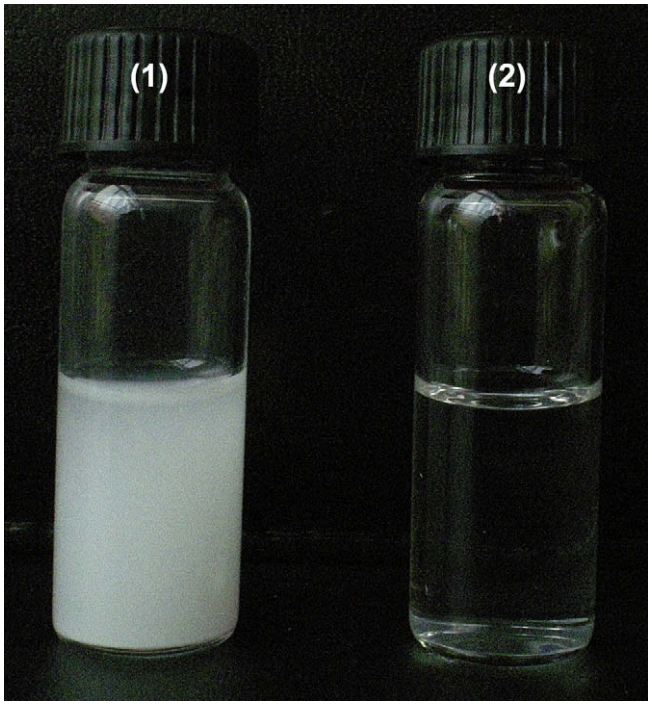

Fig. 3. Photograph of (1) as-synthesized ZrO_2/MMA dispersion and (2) MPS-functionalized ZrO_2/MMA dispersion.

Since pre-polymerization was conducted before the gel effect of polymerization occurs, the polymerization rate is dominated by the propagation rate at that stage. Therefore, reduction of propagation rate due to addition of MPS-functionalized ZrO_2 nanoparticles will ultimately lead to the decline of polymerization rate, which well explains the extended pre-polymerization time at low ZrO_2 concentration. However, at high ZrO_2 load, the desired viscosity can be reached at low monomer conversion because of the efficient crosslinking role of MPS-functionalized ZrO_2 nanoparticles. As a result, the pre-polymerization time shortens at high ZrO_2 load, despite of the reduced polymerization rate. When the ZrO_2 content is 20 wt%, the crosslinking effect is so remarkable that the polymerization reactant transforms from the desired viscosity to crosslinked gel within 10 min, which make the pre-polymerization un-controllable. Therefore, the PMMA/ZrO_2 nanocomposites with ZrO_2 content above 15 wt% was not involved, despite of the successful preparation of MMA/ZrO_2 dispersion at high ZrO_2 concentration.

The gel fraction of the nanocomposites is also listed in Table 1. It can be seen that the gel fraction reaches 72% even at 1 wt% of ZrO_2 content and is close to 100% at 5 wt% ZrO_2 content. This result indicates that the MPS-functionalized ZrO_2 nanoparticles take part in the polymerization, and as a matter of fact, act as an efficient crosslinking monomer during the polymerization of MMA.

3.3. Optical clarity of PMMA/ZrO_2 nanocomposites

Fig. 4 shows the UV–vis transmission spectra of the PMMA/ZrO_2 nanocomposite slices with different ZrO_2 contents. The figure illustrates that incorporation of ZrO_2 nanoparticles causes a slightly declined transparency relative to neat PMMA. Moreover, the transparency of the nanocomposites reduces with increasing ZrO_2 content. However, even for the nanocomposites with the lowest transparency (15 wt% ZrO_2), it still retains 86% in transmission (550 nm) relative to neat PMMA. On the contrary, the

Table 1
Polymerization results of MMA/ZrO_2 dispersions.

Sample	PMMA0	PMMA05	PMMA1	PMMA2	PMMA3	PMMA5	PMMA7	PMMA15
ZrO_2 concentration (wt%)	0	0.5	1	2	3	5	7	15
Conversion (%)	97.0	98.2	98.0	99.0	98.9	98.9	99.1	99.3
Pre-polymerization time[a] (min)	40	50	55	63	80	30	25	15
Gel fraction,%	0	42.2	72.0	82.6	93.3	98.3	98.0	99.3

[a] Note: the time to reach a viscosity of 0.9 Pa s (75 °C) at reaction temperature of 75 °C.

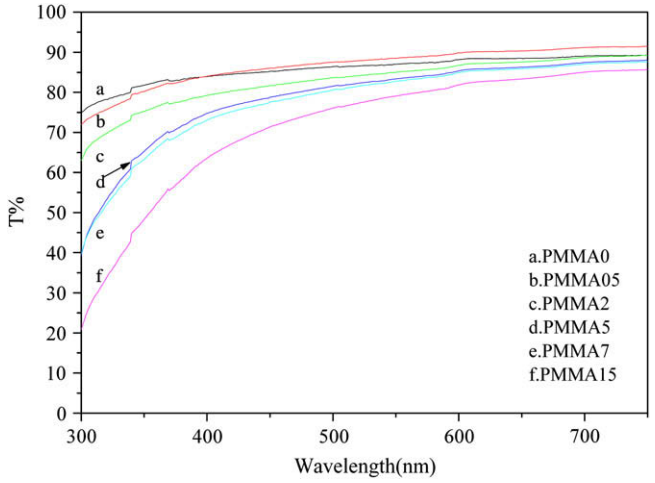

Fig. 4. UV–vis spectra of PMMA/ZrO_2 nanocomposites with various ZrO_2 contents.

transmittance of the nanocomposite slices drops drastically in the UV region as ZrO_2 content increases, suggesting the UV-blocking character of the ZrO_2 nanoparticles to some extent.

The high transparency of the nanocomposites could also be revealed from their appearances. The photographs of the typical nanocomposite slice with 15 wt% of ZrO_2 content as well as the neat PMMA slice are displayed in Fig. 5. No obvious optical difference could be distinguished with naked eyes for these two samples. The appearances of other nanocomposites are similar. So, the PMMA/ZrO_2 nanocomposites presented herein would be suitable for the fabrication of optical devices.

The high optical clarity of PMMA/ZrO_2 nanocomposites is contributed from the fine dispersion of ZrO_2 nanoparticles in the nanocomposites. Fig. 6 typically gives the TEM image of the nanocomposite with 15 wt% of ZrO_2 content. The figure clearly discloses that the ZrO_2 nanoparticles with about 4 nm of size are homogeneously dispersed in the PMMA matrix at primary particle size level.

3.4. Hardness of PMMA/ZrO_2 nanocomposites

Two kinds of tests, i.e. pendulum hardness test, nanoindentation test, were employed to determine the hardness of the PMMA/ZrO_2 nanocomposites. The pendulum hardness test is based on the principle that the amplitude of the pendulum's oscillation will decrease more quickly when supported on a softer surface, which is usually used as a measurement of the hardness of organic coatings. Fig. 7 shows the pendulum hardness of the nanocomposites as a function of ZrO_2 content. The figure clearly indicates that the pendulum hardness increases with increasing ZrO_2 content but interestingly exhibits three evolutional regions. At ZrO_2 content less than 2 wt% (Region I), the pendulum hardness quickly increases with increasing ZrO_2 content, which should be mainly due to the rapid increasing crosslinking density of the nanocomposites as shown in Table 1. However, the pendulum hardness changes a little in the range of 2–5 wt% (Region II). It could be attributed to the fact that the nearly all PMMA chains have been restricted by the ZrO_2 nanoparticles when the ZrO_2 content exceeds 2 wt%. The crosslinking cannot increase the pendulum hardness any more, and moreover, the ZrO_2 content is not high enough to cause an obvious increase of pendulum hardness. As a consequence, a plateau of pendulum hardness is observed in this range of ZrO_2 content. A considerable enhancement of pendulum hardness is observed when ZrO_2 content is continuously raised to 7 wt% and 15 wt% (Region III). The higher ZrO_2 content should be responsible for the higher pendulum hardness in this region. Therefore, for the thermoplastic polymer reinforced with inorganic nanoparticles via chemical bond interaction, the hardness of the nanocomposite would be dominated by the crosslinking density at low nanoparticle concentration level (Regions I and II) and by the volume fraction of nanoparticles at high nanoparticle concentration level (Region III).

The microhardness, marking the ability of the material's resistance to the local surface deformation, from indentation tests was listed in Table 2 for neat PMMA and PMMA/ZrO_2 nanocomposites with 5 wt% and 15 wt% of ZrO_2 content. A small increase of hardness is observed at 5 wt% of ZrO_2 content, whereas a great improvement of hardness, namely more than twofold of the

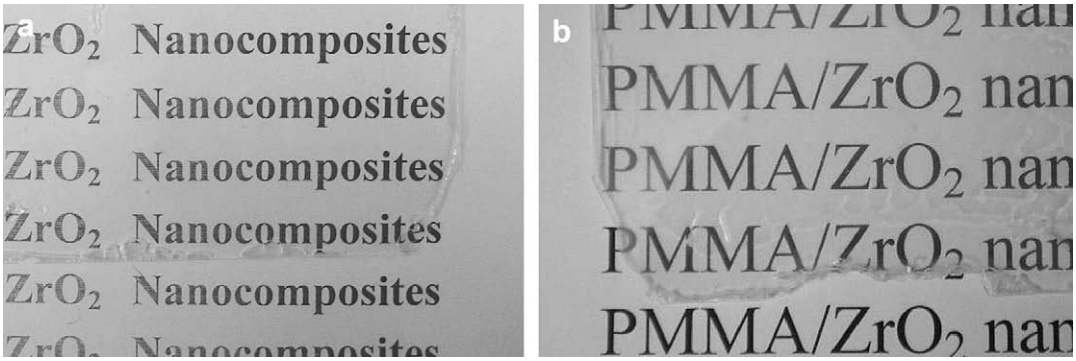

Fig. 5. Photographs of (a) neat PMMA slice (PMMA0) and (b) PMMA/ZrO_2 nanocomposite slice with 15 wt% of ZrO_2 content (PMMA15).

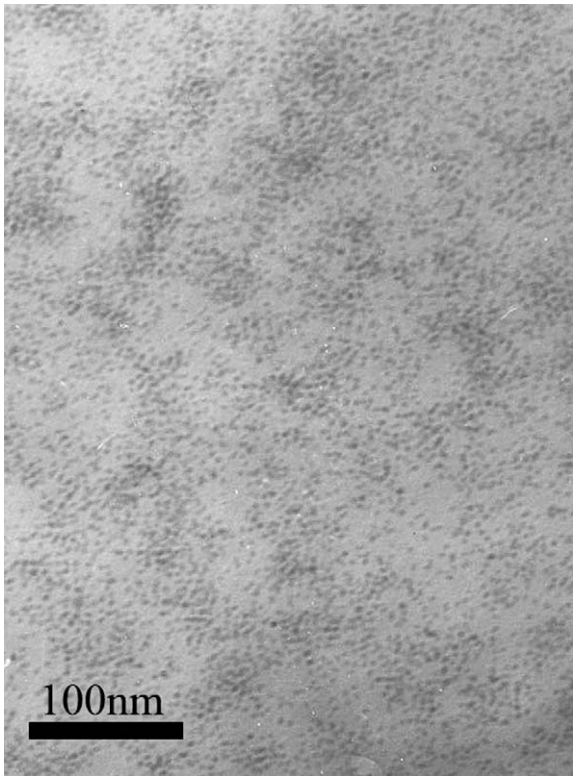

Fig. 6. TEM micrograph of PMMA/ZrO_2 nanocomposite with 15 wt% of ZrO_2 content.

hardness of neat PMMA, is attained at 15 wt% of ZrO_2 content. Therefore, both the pendulum hardness tests and indentation tests demonstrate that non-aqueous synthesized ZrO_2 nanoparticles can enhance the hardness of polymer. Nevertheless, a remarkable improvement of hardness can be achieved only at high ZrO_2 content.

The elastic modulus of the nanocomposites was also obtained from indentation tests and shown in Table 2. It increases directly with increasing ZrO_2 content, being somewhat different from the trends of microhardness. Whatever, both the microhardness and elastic modulus demonstrate the reinforcing role of ZrO_2 nanoparticles for PMMA.

Table 2
Indentation hardness of PMMA/ZrO_2 nanocomposites.

Sample name	ZrO_2 content, wt%	Microhardness, MPa	Elastic modulus, GPa
PMMA0	0	427	3.7
PMMA5	5	470	4.1
PMMA15	15	882	4.9

3.5. Scratch resistance of PMMA/ZrO_2 nanocomposites

Abrasion tests were used to simulate the anti-scratch performance of PMMA/ZrO_2 nanocomposite in real world in term of transparency reduction. The results are shown in Fig. 8. The reduction of transparency gradually decreases as the ZrO_2 content increases. Some fluctuant data are observed for the samples containing 2 wt% and 3 wt% of ZrO_2 content, which may be resulted from the measured error. The best anti-scratch performance is achieved at 15 wt% of ZrO_2 content. That is, the reduction of transparency considerably decreases from 11.8% (neat PMMA) to 3%, indicating the great improvement of scratch resistance. In comparison with the hardness results, we could find that the scratch resistance of PMMA/ZrO_2 nanocomposite is proportional to the hardness, that is, higher hardness corresponding to better scratch resistance.

Nano scratch tests were also done to evaluate the scratch resistance of PMMA/ZrO_2 nanocomposites. Fig. 9 displays the penetration depth profiles as well as the residual depth profiles for the samples PMMA0, PMMA5 and PMMA15. Some vales are clearly seen on the penetration profile curves. Careful inspection indicates that these vales are not due to the cracks that generally occur under critical load in nano scratch test of coatings, but caused by the rough surface because of the existence of apophysis and impurities on the surface of the sample, evidenced from the photograph in Fig. 10. Cracks did not actually happen in the nano scratch experiments under the applied load range for all three samples herein. Fig. 9 illustrates a slightly lower penetration depth for PMMA5 and nearly equal penetration depth for PMMA0 and PMMA15 under the same load, indicating ZrO_2 nanoparticles slightly impact the penetration depth during scratch tests. This result is somewhat deviated from the indentation test in which the microhardness obviously increases, namely the indentation depth obviously decreases, with increasing ZrO_2 content. Why the penetration depth and indentation depth of nanocomposites have different

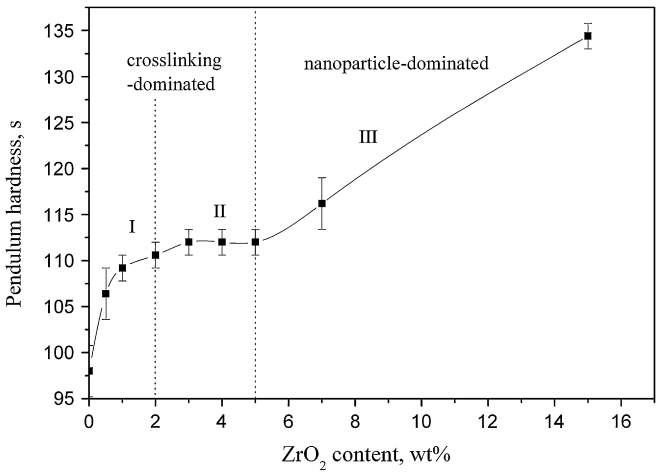

Fig. 7. Pendulum hardness of the PMMA–ZrO_2 nanocomposite slices with different ZrO_2 contents.

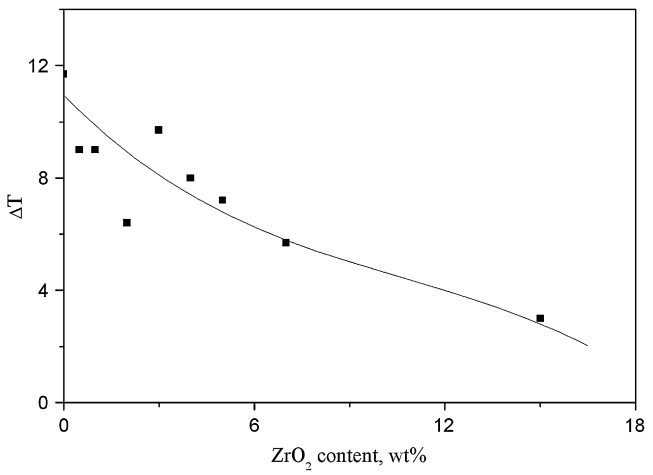

Fig. 8. The reduction of the transparency of the PMMA/ZrO_2 nanocomposite slice with different ZrO_2 contents after abrasion.

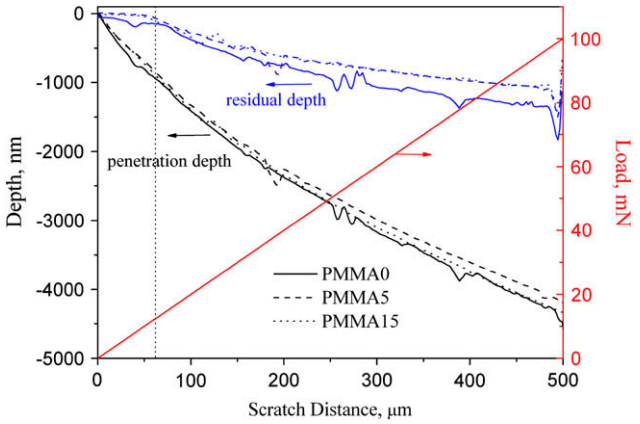

Fig. 9. Profiles of penetration depth and residual depth of PMMA0, PMMA5 and PMMA15 samples in the nano scratch tests.

trends with increasing nanoparticle content is subjected to further confirmation. As for the residual depth profiles, it can be seen that PMMA5 and PMMA15 have an overlapped curve and exhibit shallower troughs relative to PMMA after scratch. Especially at penetration depth less than about 890 nm (corresponding to 62.1 μm of scratch distance and 12.4 mN of load) the troughs completely recover, meaning that any scratch damages with the depth lower than about 1 μm will not destroy the surface of the nanocomposite. The recovery of the scratch trough is also high but not complete for pure PMMA at lower penetration depth.

The reflow capability (R) of the sample in the whole applied load range can be calculated by the equation, $R = (d_p - d_r)/d_p$, where d_p and d_r denote the penetration depth and residual depth, respectively. The calculated R values as well as their smoothed curves are plotted in Fig. 11. Except for some fluctuant R data under extremely low load (i.e. <5 mN) resulting from measured error, all curves reveal an initial decline of R with increasing load, and reach plateau R values of 0.67, 0.73 and 0.74 for PMMA0, PMMA5 and PMMA15, respectively, above load of about 25 mN. It is obvious that the R values of nanocomposites are higher than that of pure PMMA, especially in the low load range. The higher R values disclose the higher elasticity of the nanocomposites, which could be contributed from the crosslinking of PMMA chains and/or the enhanced rigidity of PMMA after incorporation of ZrO_2 nanoparticles. However, the R values are close to each other for PMMA5 and PMMA15 although PMMA15 has a much higher hardness than PMMA5 (Table 2). Recalling the fact that PMMA5 and PMMA15 have the same crosslinking degree (Table 1), it can be deduced that the elastic recovery during scratch tests is attributed to the crosslinking rather than the rigidity of the samples.

Although abrasion tests and nano scratch tests demonstrated the improved scratch resistance of PMMA via embedding with non-aqueous synthesized ZrO_2 nanoparticles, the two methods do not display the same trend on the scratch resistance of nanocomposites as a function of ZrO_2 content. PMMA15 exhibits a much better anti-scratch performance in abrasion tests but slightly better in nano scratch tests. The inconsistent results were also observed by Nothhelfer et al. [33] when they characterize the anti-scratch performance of the coatings by nano scratch experiments and Rota-Hub multi scratch tests. It is apparent that the scratch resistance result depends on the character of the probe employed [34,35]. In our experiments, the discrepancy of the scratch resistance may be owed to the different hardness of the probe. It is well known that hard material easily penetrates into soft material and causes damage of the soft material. In abrasion tests, the probe is silica-filled rubber wheels with comparable hardness as nanocomposites, and hence, a pronounced improvement of scratch resistance is manifested as the hardness of nanocomposite increases. Whereas in nano scratch tests, the probe is a diamond tip with ultrahigh hardness (~90 GPa), the increment of the hardness of PMMA/ZrO_2 nanocomposites from 0.47 GPa to 0.88 GPa is negligible in comparison with the diamond tip and thus cannot baffle the penetration of the tip to a remarkable degree. Since optical PMMA devices in real world are subjected to scratches by soft objects such as scrubbing clothes, brushes, fingers, abrasion tests would be more reliable than nano scratch tests to examine the influence of ZrO_2 nanoparticles on the scratch resistance of PMMA.

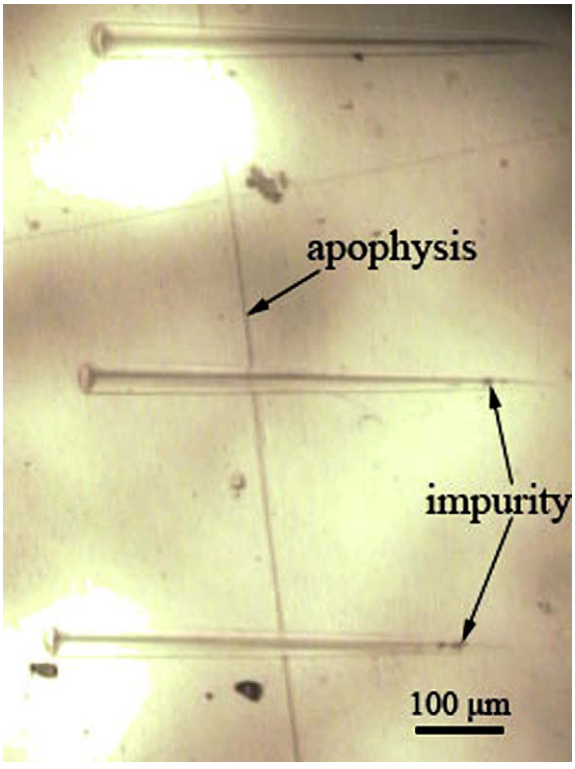

Fig. 10. Photograph of the surface of PMMA15 after nano scratch test.

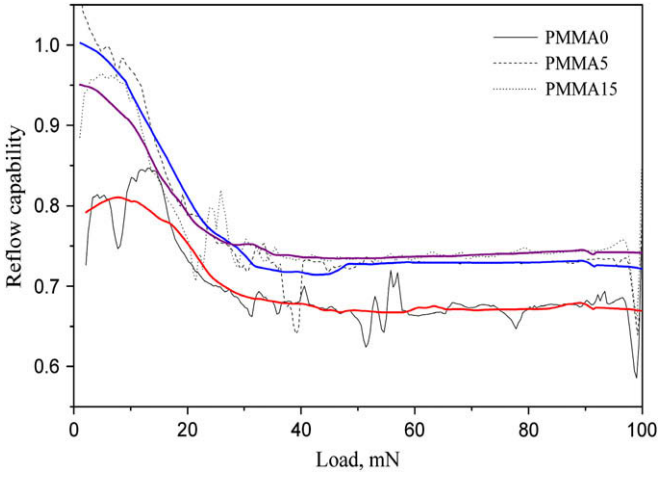

Fig. 11. Reflow capability of PMMA0, PMMA5 and PMMA15 in the nano scratch tests (thick solid lines are the corresponding smoothed curves).

4. Conclusions

Transparent PMMA/ZrO_2 nanocomposites were successfully prepared by modifying non-aqueous synthesized ZrO_2 nanoparticles in THF, dispersing MPS-functionalized ZrO_2 nanoparticles in MMA and following bulk polymerization. The MPS-functionalized ZrO_2 nanoparticles worked not only as the nanofiller but also as the efficient crosslinking monomer. PMMA completely transferred into crosslinked gel at 5 wt% of ZrO_2 content. Because of the participation of ZrO_2 nanoparticles in the polymerization of MMA, the pre-polymerization time was greatly influenced and had to be adjusted according to the ZrO_2 content. PMMA/ZrO_2 nanocomposites with high ZrO_2 content, i.e. 20 wt% and more, cannot be successfully prepared through bulk polymerization due to the serious gel effect. TEM observation indicated that ZrO_2 nanoparticles are homogeneously dispersed in PMMA matrix at primary particle size level, and therefore, leading to good transparencies of the obtained nanocomposites even at 15 wt% of ZrO_2 content.

Hardness and anti-scratch tests with various techniques revealed an interesting structure-property relationship for the PMMA/ZrO_2 nanocomposites. Due to the formation of crosslinked structure, a quick increase of pendulum hardness was observed at extremely low ZrO_2 content (i.e. 0.5 wt%). However, an obvious hardness enhancement of PMMA was realized only at high ZrO_2 content (i.e. 15 wt%), evidencing from both pendulum hardness tests and indentation tests. The abrasion tests showed a steady increment of scratch resistance of PMMA/ZrO_2 nanocomposite with increasing ZrO_2 content. The best anti-scratch performance, that is, 3.0% of the reduced percentage of transparency after abrasion test (11.8% for pure PMMA), was reached for the nanocomposite with 15 wt% of ZrO_2 content. Nevertheless, the enhancement of scratch resistance via addition of ZrO_2 nanoparticles was not pronouncedly exhibited in nano scratch tests. However, the anti-scratch improvement by the crosslinked elasticity of nanocomposite could still be sensed especially at low penetration depth. These findings would be useful in the design and characterization of nanocomposites for the cases in which inorganic nanoparticles are employed to improve the surface mechanical properties of thermoplastic polymer objects.

Acknowledgements

We are grateful for the financial support from the New Century Excellent Talent Foundation of the Ministry of Education of China (NCET-07-0210), National Nature Science Foundation (No. 50703005) of China and Shanghai Leading Academic Discipline Project (No. B113).

References

[1] Bürgel A, Kleemann W, Biebricher M, Franke H. Applied Physics A: Material Science and Processing 1995;60(5):475–80.
[2] Tsutsumi N, Ono T, Kiyotsukuri T. Macromolecules 1993;26(20):5447–56.
[3] Mustafa MD, Patrice C, Umit A, Gerhard W. Macromolecules 2007; 40(12):4190–8.
[4] Dzunuzovic E, Jeremic K, Nedeljkovic JM. European Polymer Journal 2007;43(9):3719–26.
[5] Dzunuzovic E, Marinovic-Cincovic M, Vukovic J, Jeremic K, Nedljkovic JM. Polymer Composites 2008, doi:10.1002/pc.
[6] Khaled SM, Sui RH, Charpentier PA, Rizkalla AS. Langmuir 2007; 23(7):3988–95.
[7] Mustafa MD, Mine M, Patrice C, Gerhard W. Macromolecular Rapid Communications 2006;27(10):763–70.
[8] Wang HT, Xu P, Zhong W, Shen L, Du QG. Polymer Degradation and Stability 2005;87(2):319–27.
[9] Cui LQ, Tarte NH, Woo SI. Macromolecules 2008;41(12):4268–74.
[10] Benjamin JA, Richard WS, Linda SS. Macromolecules 2004;37(4):1358–69.
[11] Avella M, Errico ME, Martuscelli E. Nano Letters 2001;1(4):213–7.
[12] Chau JLH, Hsieh CC, Lin YM, Li AK. Progress in Organic Coatings 2008;62(4):436–9.
[13] Hong RY, Fu HP, Zhang YJ, Liu L, Wang J, Li HZ, et al. Journal of Applied Polymer Science 2007;105(4):2176–84.
[14] Althues H, Palkovits R, Rumplecker A, Simon P, Sigle W, Bredol M, et al. Chemistry of Materials 2006;18(4):1068–72.
[15] Mustafa MD, Kaloian K, Umit A, Christoph B, Insun P, Ingo L, et al. Macromolecules 2007;40(4):1089–100.
[16] Aymonier C, Bortzmeyer D, Thomann R, Mulhaupt R. Chemistry of Materials 2003;15(25):4874–8.
[17] Jiang J. European Polymer Journal 2007;43(5):1724–8.
[18] Kropka JM, Putz KW, Pryamitsyn V, Ganesan V, Green PF. Macromolecules 2007;40(15):5424–32.
[19] Rosidian A, Liu YJ, Claus RO. Advanced Materials 1998;10(14):1087–91.
[20] Molina C, Moreira PJ, Gonçalves RR, SáFerreira RA, Messaddeq Y, Ribeiro SJL, et al. Journal of Materials Chemistry 2005;15(35–36):3937–45.
[21] Sangermano M, Voit B, Sordo F, Eichhorn KJ, Rizza G. Polymer 2008; 49(8):2018–22.
[22] Lee S, Shin HJ, Yoon SM, Yi DK, Choi JY, Paik U. Journal of Materials Chemistry 2008;18(15):1751–5.
[23] Zhou SX, Wu LM. Macromolecular Chemistry and Physics 2008;209(11): 1170–81.
[24] Zhou HW, Ma J, Li ZC, Chen CH. Chemical Journal of Chinese University 2005;26(8):1582–4 [in Chinese].
[25] Dey A, De SK. Journal of Applied Polymer Science 2007;105(4):2225–35.
[26] Dey A, De SK. Journal of Physics D: Applied Physics 2006;39(18):4077–86.
[27] Dey A, De SK. Journal of Nanoscience and Nanotechnology 2007;7(6):2010–5.
[28] Wang Y, Zhang DS, Shi LY, Li L, Zhang JP. Materials Chemistry and Physics 2008;110(2–3):463–70.
[29] Atik M, Luna FP, Messaddeq SH, Aegerter MA. Journal of Sol-Gel Science and Technology 1997;8(1–3):517–22.
[30] Garnweitner G, Goldenberg LM, Sakhno OV, Antonietti M, Niederberger M, Stumpe J. Small 2007;3(9):1626–32.
[31] Zhou SX, Garnweitner G, Niederberger M, Antonietti M. Langmuir 2007;23(18):9178–87.
[32] Luo KQ, Zhou SX, Wu LM, Gu GX. Langmuir 2008;24(20):11497–505.
[33] Nothhelfer-Richter R, Klinke E, Eisenbach CD. Macromolecular Symposia 2002;187(1):853–60.
[34] Wong JSS, Sue HJ, Zeng KY, Li RKY, Mai YW. Acta Materialia 2004;52(2): 431–43.
[35] Seubert CM, Nichols ME. Journal of Coatings Technology Research 2007;4(1):21–30.